Nonlinear Optical Characterization of Membrane Protein Microcrystals and Nanocrystals

7

Justin A. Newman and Garth J. Simpson

Abstract

Nonlinear optical methods such as second harmonic generation (SHG) and two-photon excited UV fluorescence (TPE-UVF) imaging are promising approaches to address bottlenecks in the membrane protein structure determination pipeline. The general principles of SHG and TPE-UVF are discussed here along with instrument design considerations. Comparisons to conventional methods in high throughput crystallization condition screening and crystal quality assessment prior to X-ray diffraction are also discussed.

Keywords

Nonlinear optical microscopy • Second harmonic generation • Two-photon excited UV fluorescence • Microscopy • High-throughput screening • Crystal detection • Crystal positioning • Crystal optimisation

7.1 Introduction

Due to the amount of time required to solve a protein structure, much effort has been placed into the optimization of the crystal structure determination pipeline. Most commonly, structure determination by crystallography begins by focusing on the selection of a suite of constructs and/or homologous targets for expression and characterization. From those, the most readily expressible, stable, biochemically active, and monodisperse candidates are prepared for crystallization screening, which typically consists of initial "sparse matrix" screens followed by refinement of conditions around the most promising positive hits. Once diffraction-quality crystals are produced, individual crystals are typically extracted into loops and cryo-cooled, followed by single-crystal X-ray diffraction at a synchrotron facility and structure determination from the resulting data. Synchrotron radiation is unique in delivering high flux with wavelength tunability, such that the large majority of high resolution protein structures generated from diffraction are now based on data acquired at synchrotron facilities (Anderson 2014; Redecke et al. 2013).

The time between the selection of an initial set of targets and the final determination of the

J.A. Newman • G.J. Simpson (✉)
Department of Chemistry, Purdue University, West Lafayette, IN 47907, USA
e-mail: newman21@purdue.edu; gsimpson@purdue.edu

I. Moraes (ed.), *The Next Generation in Membrane Protein Structure Determination*, Advances in Experimental Medicine and Biology 922, DOI 10.1007/978-3-319-35072-1_7

structure of the protein or protein complex can still be quite lengthy. Obviously, the overall duration hinges quite directly on the complexity and availability of the protein target (Skarina et al. 2014). However, there are several other bottlenecks in the current pipeline that significantly limit the throughput for obtaining a crystal structure, including screening of conditions leading to crystallization, assessment of crystal quality, and detection and location of crystals at the synchrotron (Kissick et al. 2013). The trends toward higher-throughput platforms and analysis of ever-smaller crystals is rapidly placing a greater burden on reliable, automated crystal detection.

Several relatively recent trends have aided in helping to reduce the timeframe for crystallization (Bogan 2013). Robotic and microfluidic platforms for the preparation of crystallization trials have enabled massively parallel analysis of many crystallization conditions with smaller per-trial volumes of mother liquor and less protein consumption (Zhu et al. 2014; Brodersen et al. 2013). However, highly parallel preparation substantially increases the number of wells required for inspection of crystal formation and decreases the sizes of the crystals within each lower-volume well. Automated scoring of crystallization trials based on bright field, birefringence, and ultraviolet fluorescence imaging have aided in identifying the most obvious cases of relatively large crystal formation in conventional 96 well-plate architectures, but routinely exhibit relatively high false negative rates, particularly for smaller <5–10 μm crystals. Additionally, crystallization screening can typically require several weeks to learn whether or not a particular target under a particular set of conditions will lead to protein crystal formation. The need is quickly growing for fast and reliable automated assessment of crystal formation.

However, crystal formation alone is a necessary but not always sufficient condition for structure determination. Assuming crystals can be formed, assessment of the diffraction quality of the crystals is often only meaningfully measured after extraction, cryo-cooling, and diffraction at a synchrotron facility, which can routinely require several months per iteration due to the high value of synchrotron beam time. Efforts to increase the throughput of synchrotron facilities have included fully automated systems including robotic crystal positioning and automated diffraction analyses. Similarly, reductions in the beam size have been implemented to target serial crystallography of pooled data acquired from many smaller crystals rather than one single crystal (Sanishvili et al. 2011; Wasserman et al. 2012; Mader et al. 2011). However, in both of these efforts, challenges for automated analysis rest in the need to rapidly identify crystal positions prior to data collection.

Single-shot, "diffract and destroy" methods using X-ray free electron lasers (XFEL) provides another alternative option for suspensions of many protein nanocrystals $< \sim 1$ μm in diameter (Chapman et al. 2011; Cherezov 2011), but come with even longer lead times between access to diffraction facilities, as well as challenges regarding the optimization of crystal quality for these small dimension crystals. A need for fast analysis of presence and quality of nanocrystals prior to analysis with the XFEL is quickly becoming evident as the XFEL becomes a more widely used tool for protein crystal diffraction. Based on the previously discussed trends in protein crystallography, the need is clearly growing for methods that can quickly close the feedback loops in crystal production, optimization, and X-ray data collection.

Nonlinear optical methods such as, second harmonic generation (SHG, also known as second order nonlinear optical imaging of chiral crystals, or SONICC) and two-photon excited ultra-violet fluorescence (TPE-UVF) have recently emerged as new contrast mechanisms for protein crystal detection (Kissick et al. 2009; Madden et al. 2011; Haupert et al. 2012) and are now routinely being used in the protein crystallization pipeline for high-throughput crystallization condition screening, crystal quality assessment (DeWalt et al. 2014; DeWalt et al. 2013), and detection and location of crystals in synchrotron beams (Kissick et al. 2013; Madden et al. 2013; Newman et al. 2016). The following chapter will discuss the advantages

and limitations of SHG and TPE-UVF relative to other conventional imaging techniques and describe their current role in minimizing overall timeframe for protein structure determination.

7.2 Nature of Contrast from SHG

Recently, SHG has been used as a high contrast, label-free, alternative imaging method for the detection of protein crystals (Kissick et al. 2009). SHG requires the use of a sufficiently intense light, as found in the focus of a laser, to achieve reasonably efficient nonlinear processes. As molecules approach isotropic ordering, the coherent SHG generated from the ensemble approaches zero due to internal cancellation (Boyd 2008). However, as the molecules become more ordered the SHG generated from the individual proteins constructively adds, resulting in detectable signals. SHG is strictly forbidden in centrosymmetric space groups due to the inversion symmetry cancelling out the coherent addition of SHG within the crystal. Fortuitously, the chiral nature of proteins results in crystals necessarily adopting non-centrosymmetric space groups (Haupert et al. 2012). While proteins crystallize in noncentrosymmetric space groups it is important to note that the **432** crystal class is SHG forbidden due to the high symmetry elements present in the crystal class. However, protein crystals of the **432** crystal class represent <1 % of the current PDB entries. Due to these symmetry requirements no detectable SHG is generated from amorphous aggregates that can potentially form in the crystallization of proteins. Similarly, many common salts used in the crystallization mother liquor crystallize in centrosymmetric space groups and will thus yield no signal if the salts happen to crystallize during the protein crystallization trials (Closser et al. 2013). As a result of the symmetry requirements discussed above, SHG microscopy has become a useful tool for visualizing protein crystals with many advantages over other more widely used techniques (Kissick et al. 2009).

Bright field images are sufficient for detecting large crystals in transparent media (Fig. 7.1a row 1) but suffer in translucent and turbid media (Fig. 7.1b row 1) and when the crystals are small (Fig. 7.1c row 1). Birefringence is another common imaging method used in crystal detection; however, when the sample medium is highly birefringent (Fig. 7.1b row 2) it cannot be reliably used to locate crystals. Another common technique is ultraviolet fluorescence (UVF) which uses the native autofluorescence as contrast (Vernede et al. 2006). However, UVF suffers from high background noise due to the presence of protein in solution, from protein aggregates, and from stray fluorescence from other optical elements. The resulting background can at times be sufficiently high resulting in the signal from crystals being buried in the noise. As seen in the line trace from Fig. 7.1b row 3, UVF can only detect one crystal above the noise floor, whereas the line-trace from the SHG image is able to detect multiple crystals from the same line trace with a high signal to noise ratio (SNR). The high SNR of SHG microscopy also allowed for the detection of nanocrystalline showers (Fig. 7.1c row 5) that were undetected by the other imaging techniques (Fig. 7.1c rows 1–4).

7.3 TPE-UVF vs. UVF

Fluorescent techniques have been widely used for imaging protein crystals. Conventional methods utilize a ~280 nm light source to excite tryptophan and other aromatic residues commonly found in most proteins (Judge et al. 2005). Detection of the red-shifted fluorescence allows for the localization of protein crystals within droplets. However, there are several drawbacks to imaging protein crystals by single photon UV fluorescence. The first drawback to using single photon UV fluorescence is the contribution to the background from out-of-plane signal generators such as aggregates, protein in solution, and autofluorescence from optics and the crystallization plates (Madden et al. 2011). The second drawback is the use of UV-C light. Absorption of UV-C wavelengths have been shown to break disulphide bonds, which will negatively affect the accuracy of the crystal structure that can

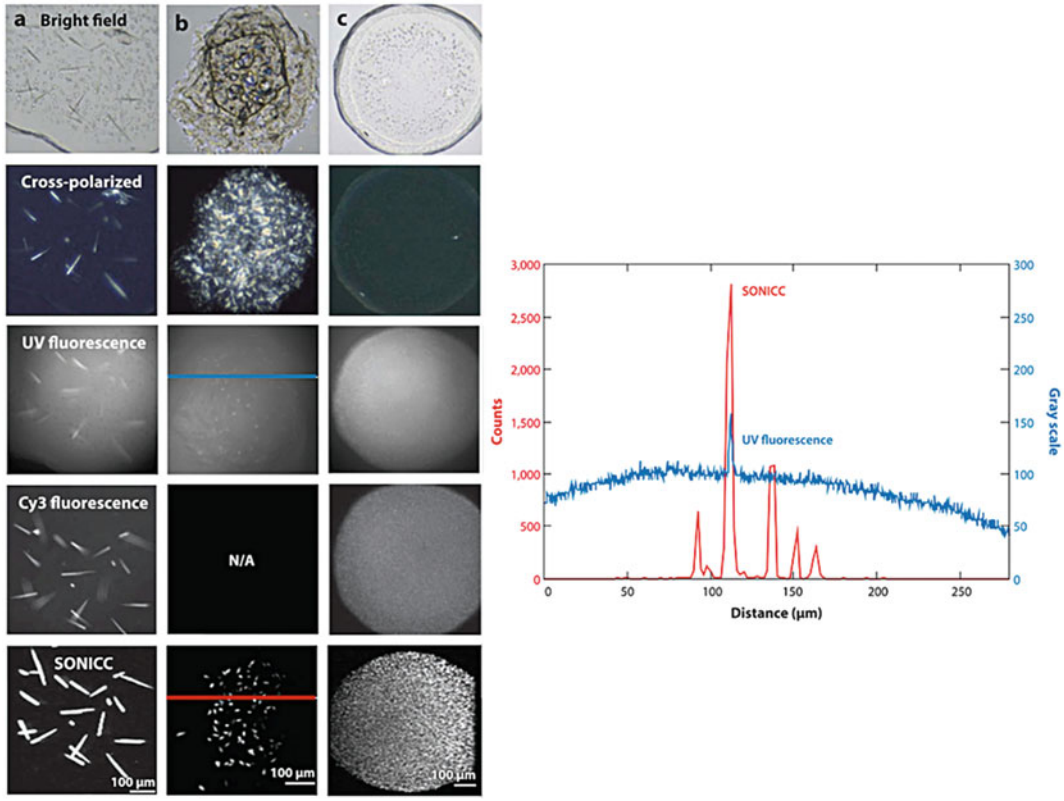

Fig. 7.1 A comparison of conventional imaging techniques along with SHG microscope images for three different samples of protein crystals grown in lipidic cubic phase (columns **a**–**c**). SHG was the only method that was able to detect the presence of crystals with high signal to noise. Line traces for fluorescence imaging and SONICC imaging shows that the significant improvement in signal to noise allows for the detection of crystals that would have otherwise gone undetected by UV fluorescence

ultimately be solved (Wien et al. 2005). Damage from these wavelengths is not limited to the focal plane, as absorption can arise with comparable efficiency above and below the focal plane as well. The operating costs for using this high energy excitation wavelength are substantially higher than those for visible wavelengths due to the need for UV transparent optics and UV transparent 96-well plates, but still relatively inexpensive.

TPE-UVF is an alternative UV fluorescence imaging method. TPE-UVF works by combining two photons of 532 nm light to excite the 266 one-photon absorption band (Madden et al. 2011). Because 2 photons of the 532 laser are required to achieve the energy required for the tryptophan residue absorption band only the most intense portion of the focus will generate the fluorescence signal. As such, this technique does not require the use of a UV light source, effectively eliminating the potential for out-of-plane sample damage and contributions to the background. This is more clearly illustrated in Fig. 7.2 comparing glucose isomerase crystals imaged by conventional single photon UV fluorescence (Fig. 7.2a) and TPE-UVF (Fig. 7.2b). Because only in-plane fluorescence is generated by TPE-UVF the image contrast is much higher for Fig. 7.2b compared to the single photon image (Fig. 7.2a) where the background has significant fluorescence contributions from out-of-plane sample.

Other nonlinear fluorescent methods have been used to image protein crystals. Native

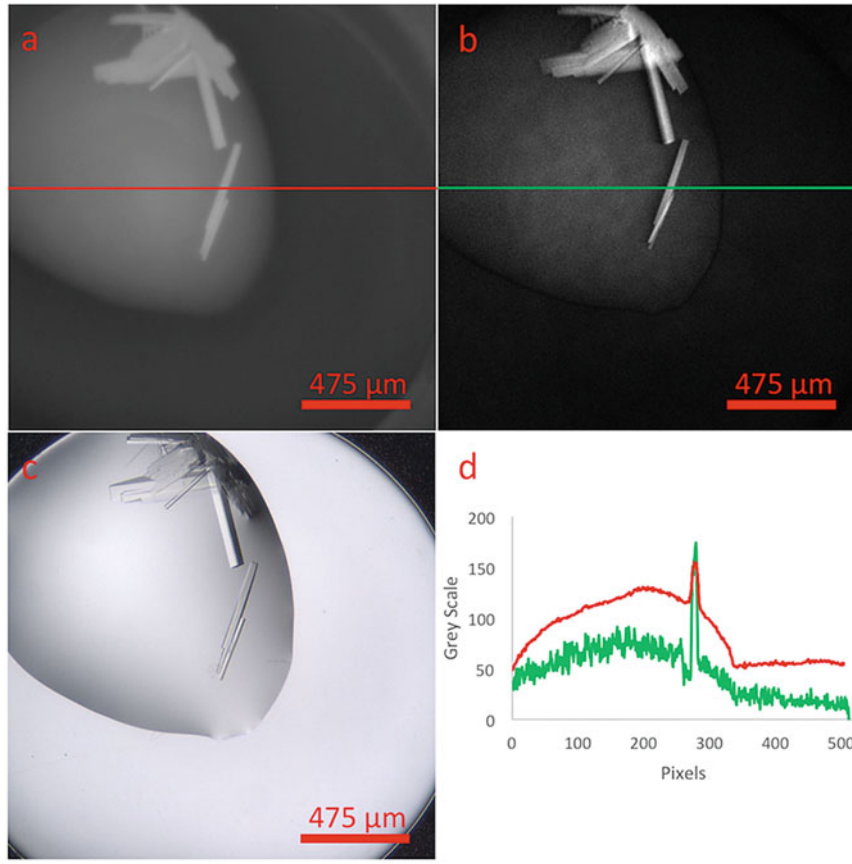

Fig. 7.2 Glucose isomerase crystals imaged by single photon UV fluorescence (**a**), two-photon excited UV fluorescence (**b**) and bright field imaging (**c**) to illustrating the improved signal to noise from the use of a two-photon process arising from the reduction in contributions to the background from out-of-plane signal generation from single photon imaging methods. A line scan is given in (**d**) to demonstrate the reduced out-of-plane signal contributions and increased SNR by using TPE-UVF

two-photon fluorescence using an excitation laser wavelength in the near IR range has been used (Padayatti et al. 2012). This method was able to easily detect protein crystals with native chromophores with absorption profiles in the 400–600 nm range. TPEF was also able to detect fluorescence from the oxidation of aromatic residues, with increases in TPEF autofluoresence signals from older proteins (>3 months). Fluorescent dyes have been used to noncovalently attach to protein crystals to increase their TPEF response (Groves et al. 2007). By using a two-photon imaging method the fluorescent background from uncrystallised protein and solvated dye was significantly reduced as compared to single photon fluorescent imaging methods.

7.4 Protein Crystal Coverage and False Negatives

7.4.1 Native SHG and TPE-UVF Protein Crystal Coverage

While SHG and TPE-UVF are capable of imaging protein crystals it is important to discuss the potential of false-positives and false-negatives. As discussed previously, SHG requires that the crystals be noncentrosymmetric to be

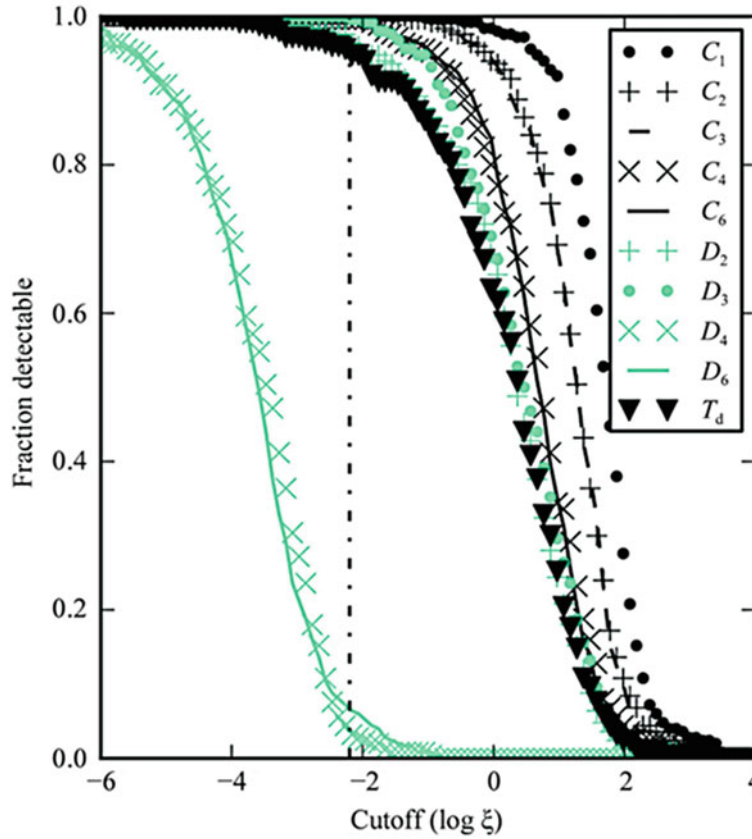

Fig. 7.3 Fraction of protein crystals detectable as a function of instrument sensitivity for different protein crystal classes. ξ is the squared magnitude of the SHG activity normalized by unit cell volume. The vertical *dashed line* represents an instrument that is sensitive enough to detect the tetragonal lysozyme polymorph with low signal to noise (ξ = 0.0064)

detectable. As a result, false-positives can arise from other noncentrosymmetric crystals that can form during a crystallization trial. While rare, a few salts commonly used in protein crystallization can generate strong SHG signals that can interfere with the SHG generated by protein crystals (Closser et al. 2013). Similarly crystals of other small molecules such as ligands can also form, leading to an increase in false-positives. Coupling SHG with other NLO techniques such as TPE-UVF reduces false-positives as most interfering salts do not exhibit fluorescence (Madden et al. 2011; Closser et al. 2013).

SHG intensity varies significantly due to crystal symmetry, with lower symmetry crystals generally exhibiting strong SHG responses compared to more symmetrical crystal lattices. Because of the variability in crystal symmetry the SHG response, from protein to protein, can span several orders of magnitude with ~84 % of the known protein data bank (PDB) entries being detectable by SHG microscopy performed with relatively long acquisition times (Haupert et al. 2012). Figure 7.3 shows the detectability of ten protein crystal classes based on the sensitivity of the instrument. The vertical dashed line represents the ability to detect tetragonal lysozyme with weak signal to noise and represents a practical lower limit for detectability. Based on this threshold greater than 90 % of all crystals in each of the eight out of ten crystal classes can be detected, however less than 10 % of protein crystals in both D_4 and D_6 crystal classes are detectable. As the measurement time is reduced, the fraction of detectable crystals will similarly decrease.

The tetragonal crystal polymorph of lysozyme is an excellent example of a crystal that is weak

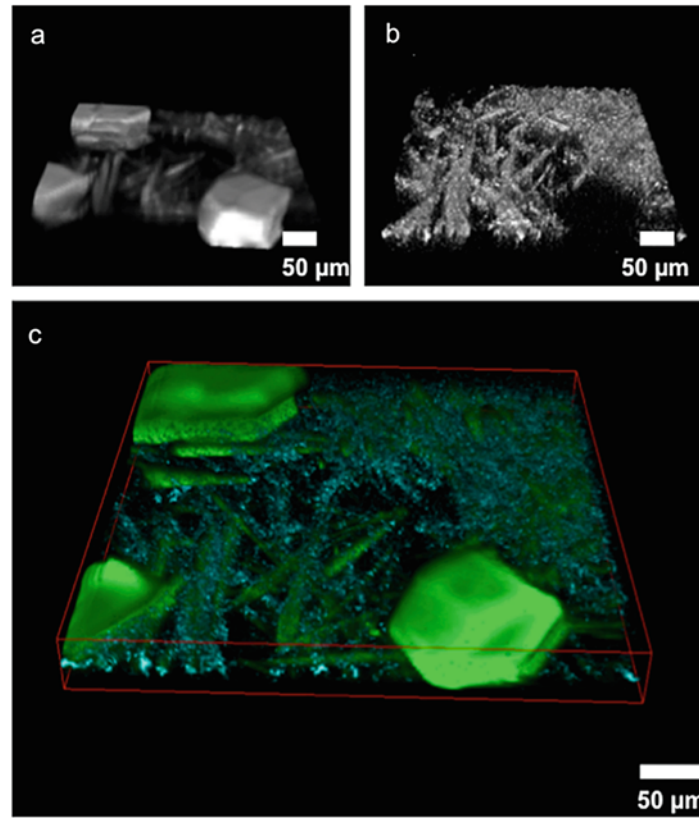

Fig. 7.4 TPE-UVF was used in panel (**a**) to detect tetragonal lysozyme polymorphs that are SHG inactive along with the SHG active monoclinic polymorphs. SHG was used in panel (**b**) to detect the SHG active monoclinic lysozyme polymorph but was unable to detect the tetragonal polymorph due to the high symmetry of the crystal lattice. The images are combined in panel (**c**)

for SHG microscopy, as seen in Fig. 7.4b. As a result of the fourfold symmetry of the $P4_32_12_1$ crystal lattice, large voids are seen in the SHG image where the crystals are located. However, SHG can readily detect the $P2_1$ lysozyme polymorph (Fig. 7.4b) (Haupert et al. 2012). Combining TPE-UVF and SHG imaging modalities onto a single imaging platform can provide complementary imaging techniques that extend the detection coverage. Because aromatic residues are commonly found in most proteins TPE-UVF is a useful method for visualizing protein crystals (Madden et al. 2011). However, like SHG, it too does not have 100 % coverage of protein crystals. There are several instances where either the lack of aromatic residues, such as in insulin, or internal fluorescence quenching, such as in catalase, limit the protein coverage for TPE-UVF (Madden et al. 2011). However, due to the presence of tryptophan in lysozyme, TPE-UVF can readily image the $P4_32_12_1$ Lysozyme polymorph, as well as the $P2_1$ polymorph (Fig. 7.4a). TPE-UVF can also be used to distinguish protein crystals from salt crystals in the rare case that the salt crystal is SHG active (Closser et al. 2013). By combining SHG and TPE-UVF in a single platform, both polymorphs of lysozyme can be detected as shown in Fig. 7.4c, and more generally an increase in protein coverage is observed.

7.4.2 Methods to Increase SHG Coverage

In an effort to increase the SHG coverage of protein crystals, a method has been developed to incorporate SHG active dyes into the crystal lattice to generate brighter SHG responses from the protein crystals (Newman et al. 2015). Unlike trace-labelling methods, which can potentially

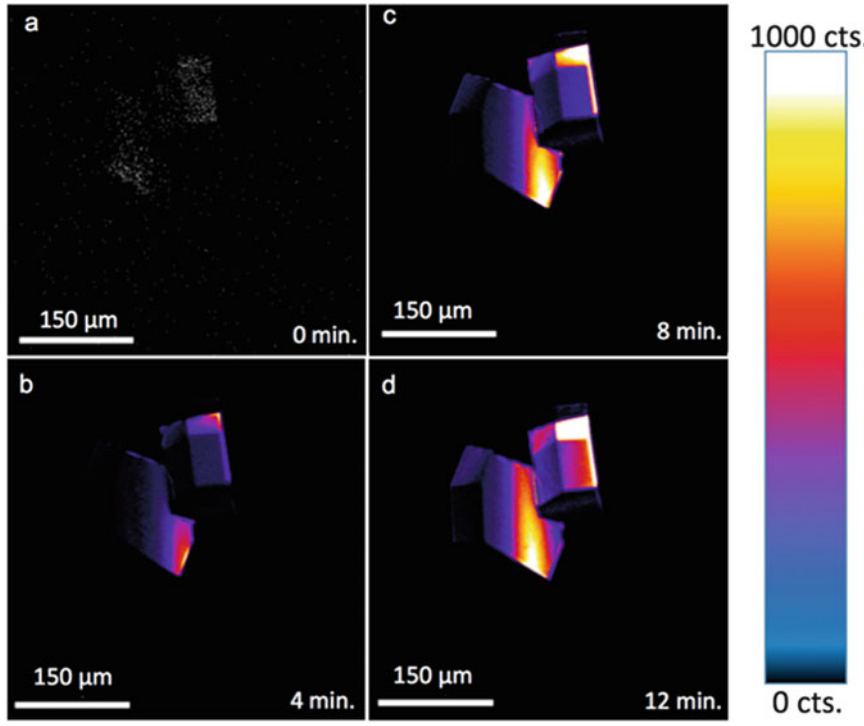

Fig. 7.5 Intercalation of 500 µM solution of malachite green into lysozyme crystals. At time zero (**a**) there is no detectable SHG. The scale was adjusted to show low counts. Within minutes detectable signal was observed (**b**–**d**) with an approximate 700-fold overall SHG enhancement after 12 min of dye intercalation

affect the protein folding (Forsythe et al. 2006), the SHG active dyes are non-covalently bound to the protein. In this method the dye can be introduced to the protein in one of two ways. First, the dye can be mixed into the mother liquor prior to crystallization. While this approach has the distinct advantage of simplicity, there is a potential risk of the dyes binding at the intermolecular contact points in the lattice, which can potentially affect crystallization. The second method is to soak the already formed crystal in a dye solution. The dye molecules intercalate into the crystal and are templated by the crystalline lattice to orient in an ordered alignment, allowing signal generation for SHG microscopy. Figure 7.5 shows the uptake of SHG active malachite green into a $P4_32_12_1$ Lysozyme crystal. After only a few minutes the SHG intensity of nominally weakly SHG-active tetragonal lysozyme (Fig. 7.5a) is increased by several orders of magnitude (Fig. 7.5b–d). By intercalating SHG active dyes into protein crystals the SHG coverage can be extended beyond the predicted 84 % coverage by native SHG. More importantly the stronger SHG signals afforded by dye intercalation allow for shorter acquisition times for improved compatibility with high-throughput crystal screening and for routine detection of nanocrystals prior to serial crystallography. However, high concentrations of dye can potentially negatively affect crystallisability (Newman et al. 2015).

7.5 Considerations for Instrument Design

7.5.1 Why Ultrafast Lasers?

The nonlinear optical methods discussed in this chapter require high optical peak powers to access efficient nonlinear optical signal generation.

However, in beam scanning microscopy, low average powers are preferred to minimize sample damage due to local heating. These dual competing criteria can be met by using an ultrafast pulsed laser (~100 fs pulses), resulting in the high peak power needed for efficient nonlinear optical generation (Haupert and Simpson 2011). As such, a 100 mW, 80 MHz laser producing 100 fs pulses generates a peak power of 12,000 W per pulse, but only over a timeframe of less than a trillionth of a second.

Several ultrafast laser sources have been used for SHG detection of protein crystals. High-powered Ti: sapphire lasers offer considerable wavelength tunability (700–1050 nm) and high average power (up to 3 W). Relatively recently, ultrafast fiber lasers have made considerable strides towards serving as viable alternatives to solid state lasers. Fiber lasers incorporate the gain medium directly into the fiber, with the fiber acting as the optical cavity of the laser. A wide variety of dopants can be used offering fixed wavelengths ranging from 1030 nm to 1550 nm. Similar to solid state lasers, average powers can reach ~1 W with 100–200 fs pulse durations in an amplified system, and several hundred mW directly from systems requiring just an oscillator. Fiber lasers, in principle, have the potential to be comparatively low cost, stable, and able to be operated hands-free (Fermann and Hartl 2009). However, the technology is still maturing and considerable variability in laser stability still exists across different systems.

7.5.2 A Beam-Scanning Approach

Nonlinear optical methods, such as SHG or TPE-UVF, most commonly produce images by focusing the laser on one pixel at a time and collecting the signal on a fast, large area photodetector, such as a photomultiplier tube (PMT). By scanning the laser across the sample, the intensity of each pixel is encoded in the time trace of the PMT response. The images can then be reconstructed by knowing which pixels correspond to which times.

There are several different methods for scanning the laser beam across the sample. Beam-scanning can either be performed by using two galvanometer-driven mirror pairs to translate the laser across the sample, or by using a slow scan galvanometer-driven mirror paired with a fast scan mirror (e.g. resonant scanner or rotating polygon). By incorporating a resonant mirror the laser can be translated rapidly (4–15 kHz) across one axis of the sample significantly reducing the pixel dwell time (Haupert and Simpson 2011). Reducing the single-pass dwell time significantly reduces potential perturbations to the sample due to local heating, allowing for higher incident powers (Fu et al. 2006). Given the nonlinear dependence of signal with peak power, the advantages of fast scanning can be quite significant. The reduction in signal due to a shorter per-pixel dwell time can be overcome by performing multiple sweeps over the same pixel to recover comparable signals generated from one inspection of a pixel with a longer dwell time.

The imaging timeframes for SHG and TPE-UVF are sufficiently short to be compatible with platforms for high throughput screening of protein crystals in 96-well plates. Using an 8 kHz resonant mirror, imaging frame rates as high as 15 frames/s (fps) can be easily realized in 512×512 imaging (Haupert and Simpson 2011), or 30 fps for bidirectional scanning. However, in high-throughput applications, a trade-off emerges between crystal detection limits and measurement time. Higher analysis speeds correspond to fewer recovered photons per crystalline sample, potentially complicating both manual and automated crystal scoring. Fortunately, the low inherent backgrounds associated with photon counting detectors allow reasonable detection of protein crystals with only a modest total number of detected photons in most instances. To achieve images with high signal-to-noise sufficient for the analysis described in the next section, longer integration times may be necessary, particularly for crystals generating weak SHG signals.

7.6 Polarization Resolved SHG for Crystal Quality Assessment

High-resolution structures determined by X-ray crystallography require diffraction from high quality protein crystals. However, determining in advance which protein crystals are of high enough quality to yield high resolution diffraction remains a difficult task. Twinned, multi-domain, or highly mosaic crystals can significantly complicate structure determination from X-ray diffraction. Twinning and multidomain crystal formation are often difficult to identify with conventional imaging techniques, since the linear optical properties are often identical for different twinned domains (Yeates and Fam 1999). *In situ* diffraction has shown some promise, but the current X-ray fluxes used do not allow for assessment of high resolution features, analysis of crystals $< \sim 10$ μm in length, or localized analysis within individual domains in larger crystals (Bingel-Erlenmeyer et al. 2011). Currently the best assessment of crystal quality comes after the crystals are extracted, cryo-cooled, and exposed to X-rays at a synchrotron source. This requirement significantly increases sample screening times at synchrotron facilities. As such, there is clearly a need for a high-throughput, non-perturbative method for assessing protein crystal quality prior to sample preparations for a synchrotron run.

The polarization-dependence of SHG provides a potential optical "handle" for initial assessments of quality for crystals still within the mother liquor. Owing to its coherent nature, the polarization state of the detected SHG signal generated from the sample is highly dependent on both the polarization state of the incident light as well as the crystal symmetry and orientation. SHG has up to 18 unique polarization-dependent tensor elements defining its orientation and polarization-dependent response, compared with just three for linear optics (Begue et al. 2009). As a result, a significantly greater amount of information is available from polarization resolved NLO measurements and analysis compared to analogous linear measurements such as birefringence.

In studies of multi-domain crystal conglomerates, polarization dependent SHG images were used to identify unique crystalline domains, confirmed by subsequent X-ray diffraction (DeWalt et al. 2013). Polarization-dependent SHG was measured by rotating waveplates to modulate the input polarization, and the polarization response was analysed by principle component analysis (PCA), shown in Fig. 7.6. The white and black portions indicate regions where the PCA determined different polarization responses, consistent with the presence of multiple domains within the crystal. X-ray diffraction measurements acquired at localized regions were consistent with a multi-domain crystal, with non-overlapping reflections arising depending on the location of diffraction.

While PCA provides some level of contrast, there are significant advantages to relating the measurements directly back to analytical models for the polarization-dependence. Nonlinear optical Stokes ellipsometry (NOSE) measurements enable the recovery of the full set of polarization-dependent free parameters available in a given sample orientation (DeWalt et al. 2014). In the case of SHG, 10 unique observables are recovered in a single measurement (5 for each detector, for vertical and horizontal detection). Once the set of free parameters is determined, the amplitudes of each coefficient can be conveniently represented as an RGBCM colour map, such that a single image per detector contains all the information from the polarization-dependent analysis. This representation also has the distinct advantage of enabling detection of multi-domain crystals based on false-colour contrast in the RGBCM maps. An obvious example is shown in Fig. 7.7b, which clearly indicates two distinct crystalline domains (Fig. 7.7a).

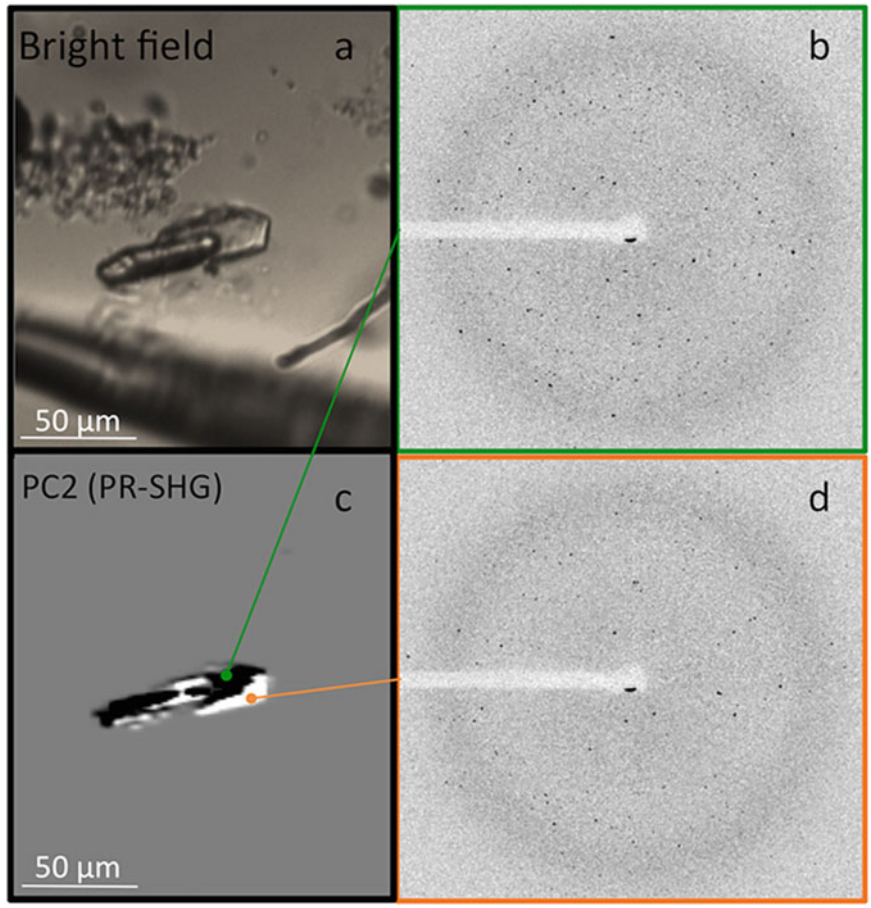

Fig. 7.6 Bright field image of a multi-domain crystal (**a**) along with the PCA image for the polarization dependent SHG signal (**c**). The white and black regions indicate locations identified by the PCA that have a different polarization response indicative of a multi-domain crystal. Diffraction from both the black (**b**) and white (**d**) region confirms the presence of multiple crystal domains

The use of an EOM allows for rapid polarization modulation (8 MHz) of the input laser resulting in the acquisition of the 5 coefficients while still maintaining video frame rates. Because of rapid data acquisition rates, the incorporation of polarization resolved SHG measurements into routine screening of crystallization trays is consistent with the timeframes typically required for high throughput SHG screening of protein crystals. Early identification of multi-domain crystals would significantly reduce the amount time spent on crystallization preparation, speed optimization, and help identify crystals likely to produce quality X-ray diffraction at synchrotron sources.

Acknowledgments The authors wish to acknowledge support from the National Institutes of Health (NIH) grants NIH-R01GM103401 and NIH-R01GM103910. We would also like to thank Ellen Gualtieri from Formulatrix for supplying the glucose isomerase crystal images in Fig. 7.2.

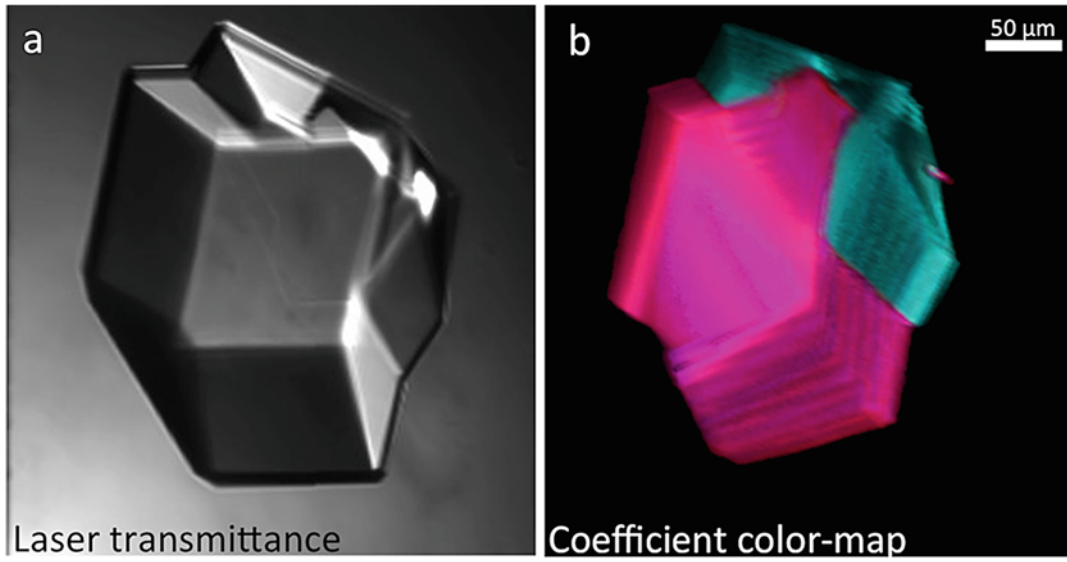

Fig. 7.7 Laser transmittance (**a**) and the coefficient colour-map (**b**) resulting from polarization resolved SHG analysis of a multi-domain glucose isomerase crystal

References

Anderson WF (2014) Structural genomics and drug discovery: methods and protocols, vol 1140. Humana Press Inc., Totowa

Begue NJ, Moad AJ, Simpson GJ (2009) Nonlinear optical stokes ellipsometry. 1. Theoretical framework. J Phys Chem C 113(23):10158–10165

Bingel-Erlenmeyer R, Olieric V, Grimshaw JPA, Gabadinho J, Wang X et al (2011) SLS crystallization platform at beamline X06DA—a fully automated pipeline enabling in situ X-ray diffraction screening. Cryst Growth Des 11(4):916–923

Bogan MJ (2013) X-ray free electron lasers motivate bioanalytical characterization of protein nanocrystals: serial femtosecond crystallography. Anal Chem 85(7):3464–3471

Boyd RW (2008) Nonlinear optics, 3rd edn. Elsevier Inc, Cambridge

Brodersen DE, Andersen GR, Andersen CBF (2013) Mimer: an automated spreadsheet-based crystallization screening system. Acta Crystallogr F Struct Biol Commun Acta 69(7):815–820

Chapman HNF, Fromme P, Barty A, White TA, Kirian RA et al (2011) Femtosecond X-ray protein nanocrystallography. Nature 470:73–77

Cherezov V (2011) Lipidic cubic phase technologies for membrane protein structural studies. Curr Opin Struct Biol 21:559–566

Closser RG, Gualtieri EJ, Newman JA, Simpson GJ (2013) Characterization of salt interferences in second-harmonic generation detection of protein crystals. J Appl Crystallogr 46(6):1903–1906

DeWalt EL, Begue VJ, Ronau JA, Sullivan SZ, Das C, Simpson GJ (2013) Polarization-resolved second-harmonic generation microscopy as a method to visualize protein-crystal domains. Acta Crystallogr D Biol Crystallogr 69(1):74–81

DeWalt EL, Sullivan SZ, Schmitt PD, Muir RD, Simpson GJ (2014) Polarization-modulated second harmonic generation ellipsometric microscopy at video rate. Anal Chem 86(16):8448–8456

Fermann ME, Hartl I (2009) Ultrafast fiber laser technology. IEEE J Sel Top Quantum Electron 15(1):191–206

Forsythe E, Achari A, Pusey ML (2006) Trace fluorescent labeling for high-throughput crystallography. Acta Crystallogr D Biol Crystallogr 62(3): 339–346

Fu Y, Wang H, Shi R, Cheng J-X (2006) Characterization of photodamage in coherent anti-Stokes Raman scattering microscopy. Opt Express 14(9):3942–3951

Groves MR, Muller IB, Kreplin X, Muller-Dieckmann J (2007) A method for the general identification of protein crystals in crystallization experiments using a noncovalent fluorescent dye. Acta Crystallogr D Biol Crystallogr 63(4):526–535

Haupert LM, Simpson GJ (2011) Screening of protein crystallization trials by second order nonlinear optical imaging of chiral crystals (SONICC). Methods 55(4):379–386

Haupert LM, DeWalt EL, Simpson GJ (2012) Modeling the SHG activities of diverse protein crystals. Acta Crystallogr D Biol Crystallogr 68(11):1513–1521

Judge RA, Swift K, Gonzalez C (2005) An ultraviolet fluorescence-based method for identifying and distinguishing protein crystals. Acta Crystallogr D Biol Crystallogr 61(1):60–66

Kissick DJ, Gualtieri EJ, Simpson GJ, Cherezov V (2009) Nonlinear optical imaging of integral membrane protein crystals in lipidic mesophases. Anal Chem 82(2):491–497

Kissick DJ, Dettmar CM, Becker M, Mulichak AM, Cherezov V et al (2013) Towards protein-crystal centering using second-harmonic generation (SHG) microscopy. Acta Crystallogr D Biol Crystallogr D 69(5):843–851

Madden JT, DeWalt EL, Simpson GJ (2011) Two-photon excited UV fluorescence for protein crystal detection. Acta Crystallogr D Biol Crystallogr 67(10): 839–846

Madden JT, Toth SJ, Dettmar CM, Newman JA, Oglesbee RA, Hedderich HG, Everly RM, Becker M, Ronau JA, Buchanan SK et al (2013) Integrated nonlinear optical imaging microscope for on-axis crystal detection and centering at a synchrotron beamline. J Synchrotron Radiat 20(4):531–540

Mader K, Marone F, Hintermuller C, Mikuljan G, Isenegger A, Stampanoni M (2011) High-throughput full-automatic synchrotron-based tomographic microscopy. J Synchrotron Radiat 18(2):117–124

Newman JA, Scarborough NM, Pogranichniy NR, Shrestha RK, Closser RG, Das C, Simpson GJ (2015) Intercalating dyes or enhanced contrast in second harmonic generation imaging of protein crystals. Acta Crystallogr D Biol Crystallogr 71(7): 1471–1477

Newman JA, Zhang S, Sullivan SZ, Dow XY, Becker M, Sheedlo MJ, Stepanov S, Carlsen MS, Everly RM, Das C et al (2016) Guiding synchrotron Xray diffraction by multimodal video-rate protein crystal imaging. J Synchrotron Radiat 23(4)

Padayatti P, Palczewska G, Sun W, Palczewski K, Salom D (2012) Imaging of protein crystals with two-photon microscopy. Biochemistry 51(8):1625–1637

Redecke L, Nass K, DePonte DP, White TA, Rehders D et al (2013) Natively inhibited Trypanosoma brucei Cathepsin B structure determined by using an X-ray laser. Science 339:227–230

Sanishvili R, Yoder DW, Pothineni SB, Rosenbaum G, Xu S, Vogt S, Stepanov S, Makarov OA, Corcoran S, Benn R et al (2011) Radiation damage in protein crystals is reduced with a micron-sized X-ray beam. Proc Natl Acad Sci U S A 108(15):6127–6132

Skarina T, Xu X, Evdokimova E, Savchenko A (2014) High-throughput crystallization screening. Methods Mol Bio 1140:159–168

Vernede X, Lavault B, Ohana J, Nurizzo D, Joly J et al (2006) UV laser-excited fluorescence as a tool for the visualization of protein crystals mounted in loops. Acta Crystallogr D Biol Crystallogr 62(3): 253–261

Wasserman SR, Koss JW, Sojitra ST, Morisco LL, Burley SK (2012) Rapid-access, high-throughput synchrotron crystallography for drug discovery. Trends Pharmacol Sci 33(5):261–267

Wien F, Miles AJ, Lees JG, Vronning Hoffmann S, Wallace BA (2005) VUV irradiation effects on proteins in high-flux synchrotron radiation circular dichroism spectroscopy. J Synchrotron Radiat 12(4): 517–523

Yeates TO, Fam BC (1999) Protein crystals and their evil twins. Structure 7(2):R25–R29

Zhu Y, Zhu L-N, Guo R, Cui H-J, Ye S, Fang Q (2014) Nanoliter-scale protein crystallization and screening with a microfluidic droplet robot. Sci Rep 4:5046